

Supplemental Information - Glassy Dynamics in Composite Biopolymer Networks

Tom Golde,¹ Constantin Huster,² Martin Glaser,^{1,3} Tina Händler,^{1,3}

Harald Herrmann,^{4,5} Josef A. Käs,¹ and Jörg Schnauß^{1,3}

¹*Peter Debye Institute for Soft Matter Physics,
University of Leipzig, 04103 Leipzig, Germany*

²*Institute for Theoretical Physics, University of Leipzig, 04103 Leipzig, Germany*

³*Fraunhofer Institute for Cell Therapy and Immunology, 04103 Leipzig, Germany*

⁴*Molecular Genetics, German Cancer Research Center, 69120 Heidelberg, Germany*

⁵*Department of Neuropathology, University Hospital Erlangen, 91054, Erlangen, Germany*

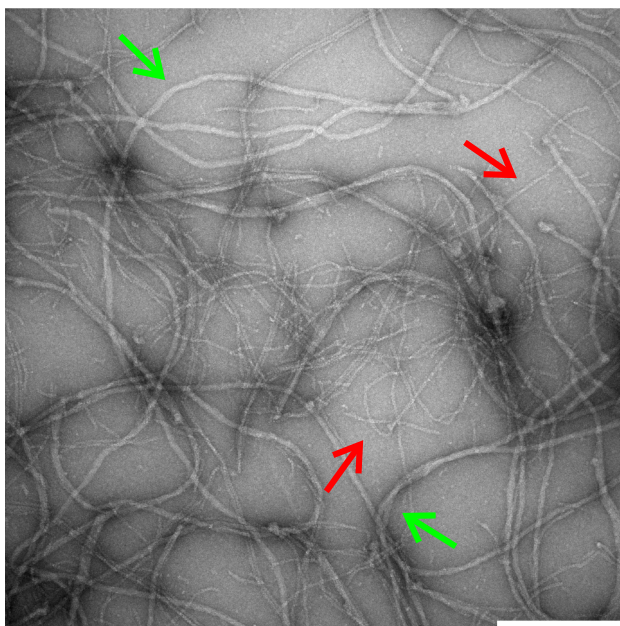


Figure S1. The transmission electron microscopy image of a composite actin/vimentin network illustrates that both biopolymers co-polymerize under the same conditions (here polymerization for 20 min at 37 °C) forming an interwoven network, which was subsequently fixed with Glutaraldehyde for imaging. Arrow heads indicate single actin (red) and vimentin (green) filaments. The scale bar is 200 nm.

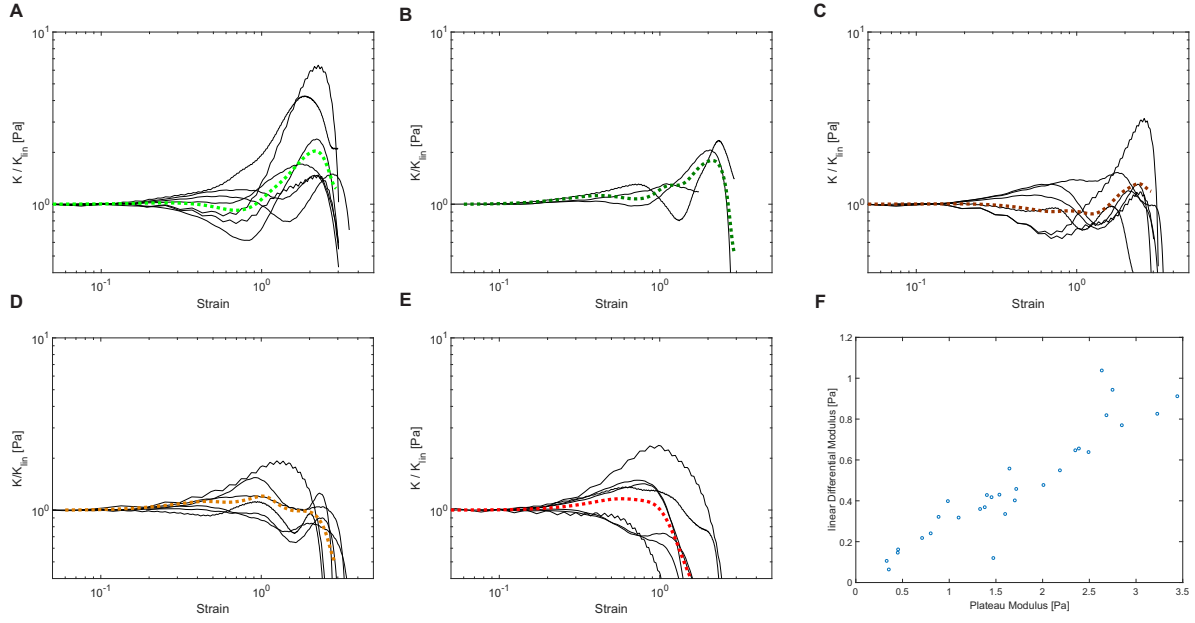


Figure S2. Differential shear modulus K rescaled by its linear value K_{lin} versus strain for different network compositions. Thick dashed lines are obtained from the mean stress-strain curves. (A), vimentin 1 g/l. (B), vimentin 0.75 g/l actin 0.125 g/l. (C), vimentin 0.5 g/l actin 0.25 g/l. (D), vimentin 0.25 g/l actin 0.375 g/l. (E), actin 0.5 g/l. (F), Linear differential shear modulus K_{lin} versus plateau modulus $G_0 = G'(f = 1 \text{ Hz})$.

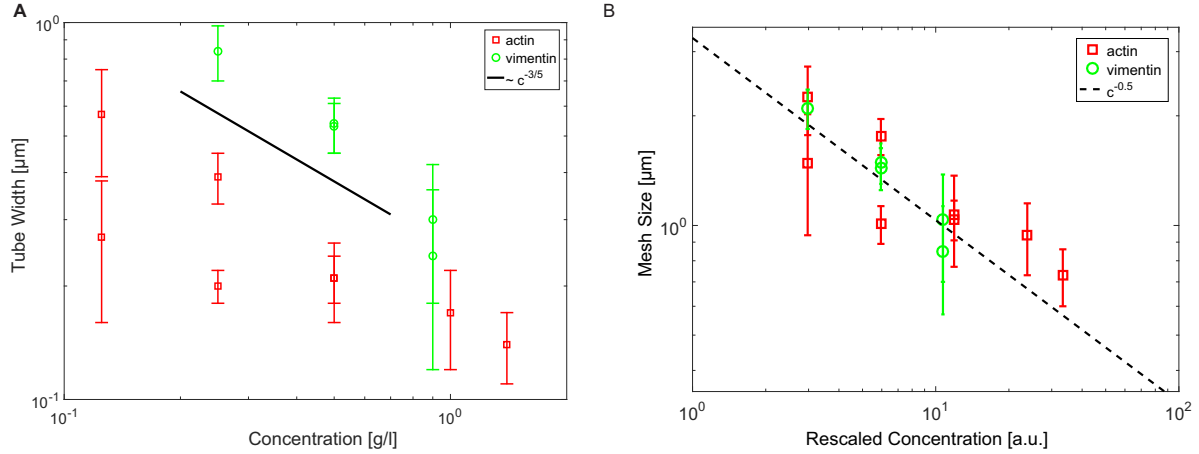


Figure S3. (A), Shown is the tube width versus concentration in pure actin (red) and pure vimentin (green) networks with the black line indicating the scaling predicted by the tube model with a power law exponent of $-3/5$. (B), Mesh size versus rescaled concentration in pure actin (red) and pure vimentin (green) networks are displayed with black dashed line indicating the scaling predicted by the tube model with a power law exponent of -0.5 . Data points in A and B are the weighted mean of all filaments within one sample. Error bars represent the standard deviation of the weighted mean.

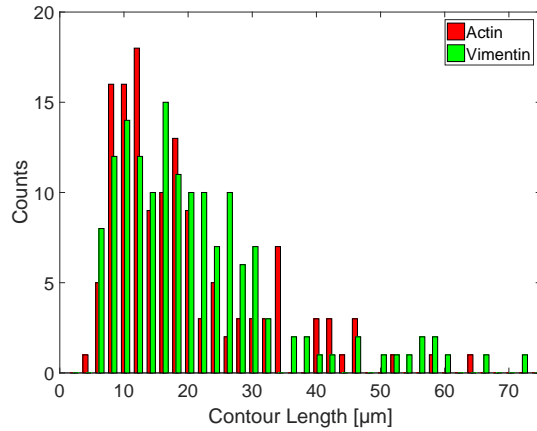


Figure S4. Length distribution of the fluorescently labeled actin and vimentin filaments in the composite and pure actin and vimentin samples presented in Fig. 2B in the main text. The number of filaments is $n = 136$ for F-actin and $n = 153$ for vimentin IF.

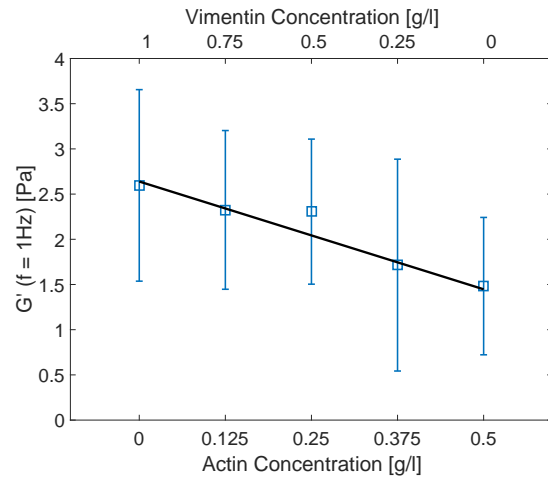


Figure S5. Pseudo plateau modulus $G_0 = G'(f = 1 \text{ Hz})$. Data points are the mean values with standard deviation. Black line are the results from the superposition described by Eq. 4 in the main text.

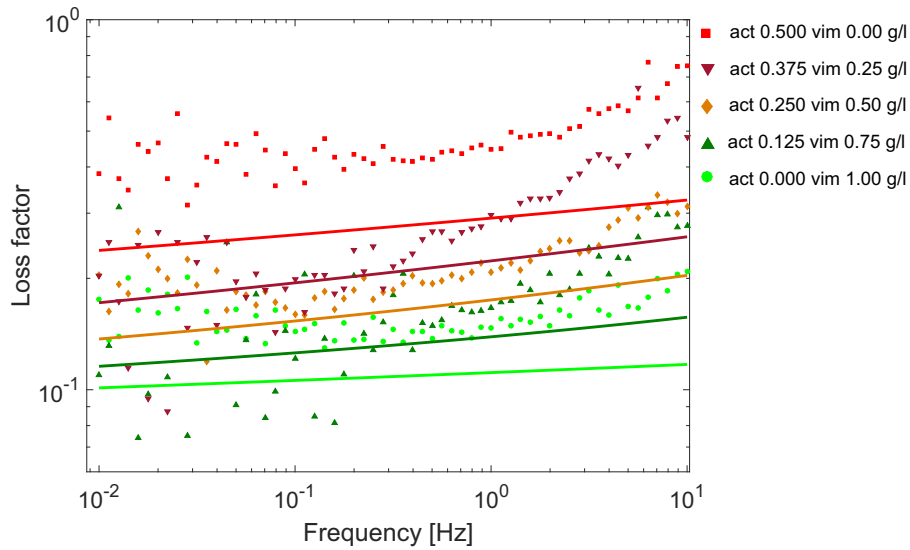


Figure S6. Loss factor $\tan(\phi) = G''/G'$ over frequency. Data points are the mean values of all measurements. Straight lines are the results of the GWLC fits.

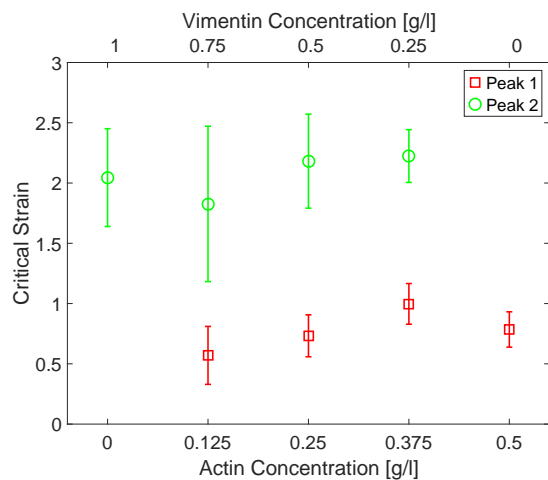


Figure S7. Critical strain γ_{crit} defined as the strain of a peak in the differential modulus K . Data points are the mean values with standard deviation. Peak 1 in composite network is defined as the peak with the smaller γ_{crit} . This shows, that peak 1 can be attributed to the underlying F-actin network while peak 2 can be attributed to the underlying vimentin IF network.

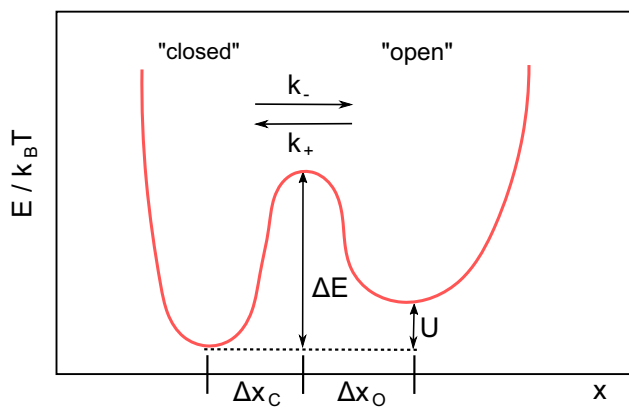


Figure S8. Sketch of the bimodal energy-landscape used for modeling weak reversible binding mechanisms. To transition from the closed to the open state, an energy barrier of height ΔE has to be overcome.

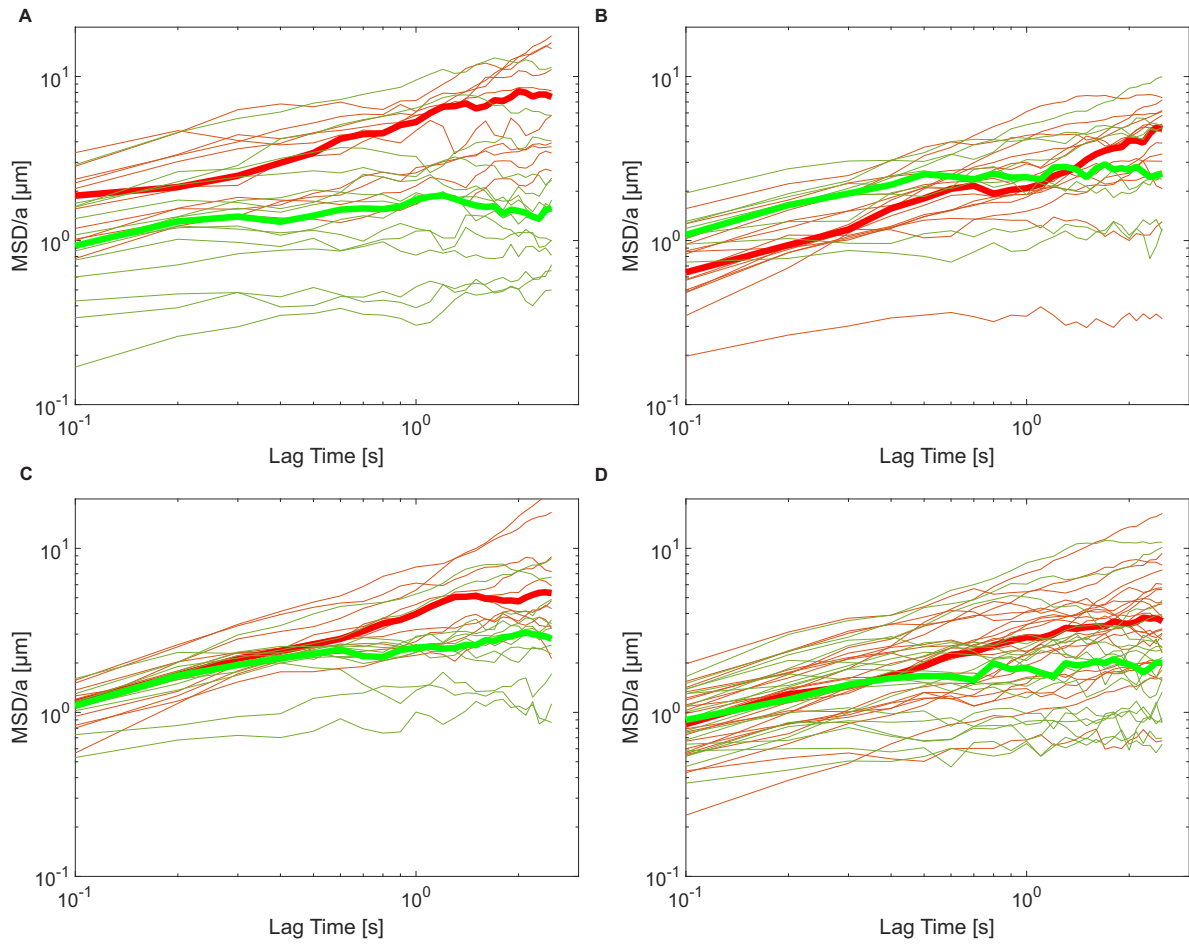


Figure S9. MSD of the filament center parallel to the tube for actin (dark red) and vimentin (dark green) filaments rescaled by the tube width a . Thick lines are the median of all actin (red) and vimentin (green) filaments of the respective network composition. (A) Pure actin at 0.5 g/l and pure vimentin at 1 g/l, (B) actin 0.125 g/l vimentin 0.75 g/l, (C) actin 0.25 g/l vimentin 0.5 g/l, and (D) actin 0.375 g/l vimentin 0.25 g/l.

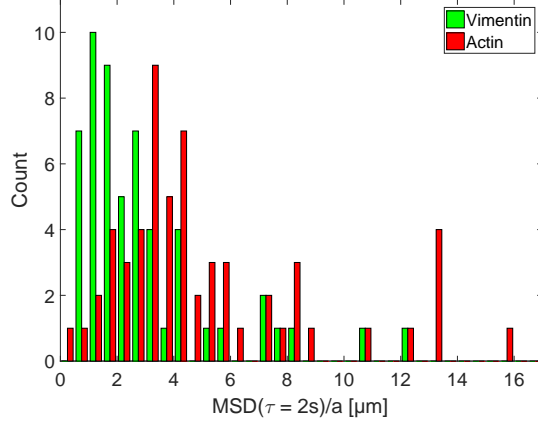


Figure S10. Histogram of the MSD at a lag time $\tau = 2$ s rescaled by tube width a of the actin and vimentin filaments in composite and pure actin and vimentin networks presented in Fig. 5 of the main text. The median $\text{MSD}(\tau = 2\text{s})/a$ is $4.1 \mu\text{m}$ for F-actin with $n = 59$ and $2.0 \mu\text{m}$ for vimentin IF with $n = 55$. Despite a strong filament to filament variation, both distributions are significantly different with $p = 9 \times 10^{-6}$ obtained from a Kolmogorow-Smirnow test.

linear rheology:		
temperature	T	293 K
contour length actin	L	$16 \mu\text{m}$
contour length vimentin	L	$18 \mu\text{m}$
persistence length actin	l_p	$10 \mu\text{m}$
persistence length vimentin	l_p	$2 \mu\text{m}$
drag coefficient per length	ζ_{\perp}	$2 \text{ mPa}\cdot\text{s}$
mesh size of the pure networks	ξ_0	$1 \mu\text{m}$
non-linear rheology:		
characteristic width of a free energy well	δ	0.9 nm
energy difference between the bound and the unbound state	U	$2.5 k_B T$
control parameter for filament lengthening	S	0.3
distance between bound and unbound state	Δx	2 nm

Table S I. Fixed parameters for the description of the linear rheology and non-linear rheology.

SI TEXT

The glassy wormlike chain

For the theoretical description of the measured data we used the glassy wormlike chain model (GWLC) [1]. As a simple extension of a standard polymer model – the wormlike chain (WLC) – the GWLC describes the time-dependent rheological properties of cells as well as semiflexible polymer networks by modeling the interactions of a test chain with its soft environment via an exponential stretching of the WLC mode relaxation spectrum. In particular the WLC mode relaxation times $\tau_n^{\text{WLC}} = \zeta_{\perp}/(\kappa\pi^4/\lambda_n^4 + f\pi^2/\lambda_n^2)$ are stretched according to:

$$\tau_n^{\text{GWLC}} = \begin{cases} \tau_n^{\text{WLC}} & \text{if } \lambda_n \leq \Lambda \\ \tau_n^{\text{WLC}} e^{\varepsilon N_n} & \text{if } \lambda_n > \Lambda. \end{cases} \quad (1)$$

Here, $\lambda_n = L/n$ is the (half-) wavelength of the n -th mode, L the contour length of the test filament, Λ the typical distance between two interactions, f describes a homogeneous backbone tension accounting for existing pre-stress, ζ_{\perp} the transverse drag coefficient, and κ the bending rigidity which is related to the filament's persistence length l_p via $\kappa = l_p k_B T$. The number $N_n = \lambda_n/\Lambda - 1$ of interaction points associated to the n -th mode is set to 0 for modes shorter than Λ . ε is the stretching parameter controlling how strong the modes are slowed down by interactions with the environment.

The physical picture behind this scheme is that of a test polymer diffusing in a rough free energy landscape created by the surrounding polymers. In this picture the interactions correspond to the wells of this landscape separated by energy barriers of typical height ε . The GWLC mode relaxation spectrum given in equation 1 can then be introduced in a consistent way by assuming that in the considered free energy landscape the mode-number-dependent friction is given by:

$$\zeta_{\perp}(n) = \begin{cases} \zeta_{\perp} & \text{if } \lambda_n \leq \Lambda \\ \zeta_{\perp} e^{\varepsilon N_n} & \text{if } \lambda_n > \Lambda. \end{cases} \quad (2)$$

Linear rheology

In the frequency domain, the micro-rheological, linear response function $\chi(\omega)$ of the GWLC to a point force at its ends can be expressed as the sum of mode contributions:

$$\chi(\omega) = \frac{L^4}{\pi^4 l_p^2 k_B T} \sum_{n=1}^{\infty} \frac{1}{(n^4 + n^2 f/f_E) (1 + i\omega\tau_n^{\text{GWLC}}/2)}. \quad (3)$$

From $\chi(\omega)$, the complex linear modulus $G^*(\omega)$ in the high frequency limit can be obtained assuming affine deformations:

$$G^*(\omega) = \frac{\Lambda}{5\xi^2\chi(\omega)}. \quad (4)$$

Within these expressions, $f_E = \kappa\pi^2/L^2$ is the Euler buckling force and ξ denotes the mesh size. The sum converges rapidly for $\lambda_n > \Lambda$ so that high precision can be obtained by adding a small number of mode contributions.

Non-linear rheology

To model inelastic filament lengthening, we assume that the increase of the filaments contour length is related to a slippage of proto-filaments, which requires the opening of transient bonds between proto-filaments or the unfolding of protein domains. Following standard procedures [2] based on the Bell-Evans-model [3], we represent the force dependent dynamics of such weak reversible binding mechanisms (to which we refer as bonds) via a first order rate equation for the time dependent probability $\nu(t, f)$ that a bond is found in the closed state in the presence of an external force f :

$$\dot{\nu}(t, f) = -k_-(f)\nu(t, f) + k_+(f)(1 - \nu(t, f)), \quad (5)$$

where the force dependency of the transition rates $k_-(f)$ and $k_+(f)$ is chosen according to the Bell model [4]:

$$k_-(f) = k_0 \cdot e^{\Delta E + \beta \Delta x_c f} \quad (6)$$

$$k_+(f) = k_0 \cdot e^{\Delta E - \beta \Delta x_o f + U}, \quad (7)$$

where k_0 is a microscopic attempt rate. The underlying picture of this description bonds is an ensemble of virtual particles diffusing in an asymmetric bimodal potential (Fig. S6). The two energy minima at $x = 0$ and $x = \Delta x_o + \Delta x_c$ describe the closed and the open state of

the bond, respectively. The energetic minimum representing the closed state minimum is set to zero and that of open state to U . The two minima are separated by an energy barrier of height ΔE at $x = \Delta x_c$.

To link $\nu(t, f)$ to the GWLC we replace the constant contour length L by a contour length $L(\nu(t, f))$ that depends on the state of the bonds. In particular we choose a linear coupling:

$$L \rightarrow L(\nu_\infty(t, f)) = L_0 [1 + \mathcal{S}(\nu_\infty(0, 0) - \nu_\infty(t, f))], \quad (8)$$

where \mathcal{S} is the coupling constant. This simplifying ansatz (Eq. 8) rests on the assumption that $L(\nu_\infty(t, f))$ has the character of a slow variable. It is employed because here, we are only interested in a minimal description whereas the full problem of combining a description of a weak reversible binding mechanism with a polymer model on microscopic grounds is in general very complicated and beyond the scope of this paper.

Further we consider only the limit of an externally applied forces changing slowly compared to $1/(k_0 \exp(\Delta E))$ so that $\nu(t, f)$ has enough time to equilibrate and thus, is well approximated by the time-independent equilibrium value $\nu_{\text{eq}}(f)$:

$$\nu_{\text{eq}}(f) = (1 + \exp[-U + \Delta x f])^{-1}, \quad (9)$$

with $\Delta x = \Delta x_c + \Delta x_o$. Combining Eq. 9 with Eq. 8 yields an expression for a force-dependent filament length $L(f)$ then reads:

$$L(f) = L_0 \left[1 + \frac{S \cdot \sinh(f \Delta x / 2)}{\cosh(U - f \Delta x / 2) + \sinh(f \Delta x / 2)} \right]. \quad (10)$$

which can be plugged in the description of the differential modulus described above. The resulting differential modulus then shows an initial softening regime, caused by an increasing $L(f)$ as observed in the experiments.

SUPPORTING REFERENCES

- [1] K. Kroy and J. Glaser, *New J. Phys.*, 2007, **9**, 416.
- [2] L. Wolff, P. Fernandez and K. Kroy, *New J. Phys.*, 2010, **12**, 053024.
- [3] E. Evans and K. Ritchie, *Biophys. J.*, 1997, **72**, 1541–1555.
- [4] G. I. Bell *et al.*, *Science*, 1978, **200**, 618–627.